Available online at www.sciencedirect.com
ScienceDirect
Advances in Water Resources 30 (2007) 794–807
Advances in Water Resources
www.elsevier.com/locate/advwatres

Non-passive transport of volatile organic compounds in the unsaturated zone

Orlando Silva, Jordi Grifoll *

Grup de recerca de Fenòmens de Transport, Departament d'Enginyeria Química, Universitat Rovira i Virgili, Av. dels Països Catalans 26, 43007 Tarragona, Spain

Received 16 December 2005; received in revised form 6 June 2006; accepted 15 June 2006
Available online 17 August 2006

Abstract

A detailed model was formulated to describe the non-passive transport of water-soluble chemicals in the unsaturated zone and used to illustrate one-dimensional infiltration and redistribution of alcohol–water mixtures. The model includes the dependence of density, viscosity, surface tension, molecular diffusion coefficient in the liquid-phase, and gas–liquid partition coefficient on the aqueous mixture composition. It also takes into account the decrease in the gas–liquid partition coefficient at high capillary pressures, in accordance with Kelvin's equation for multi-component mixtures. Simulation of butanol–water mixtures infiltration in sand was in agreement with the experimental data and simulations reported in the literature. Simulation of methanol infiltration and redistribution in two different soils showed that methanol concentration significantly affects volumetric liquid content and concentration profiles, as well as the normalized volatilization and evaporation fluxes. Dispersion in the liquid-phase was the predominant mechanism in the transport of methanol when dispersivity at saturation was set to 7.8 cm. Liquid flow was mainly due to capillary pressure gradients induced by changes in volumetric liquid content. However, for dispersivity at saturation set to 0.2 cm, changes in surface tension due to variation in composition induced important liquid flow and convection in the liquid-phase was the most active transport mechanism. When the Kelvin effect was ignored within the soil, the gas-phase diffusion was significantly lower, leading to lower evaporation flux of water and higher volumetric liquid contents near the soil surface.

Keywords: Solute transport; VOC transport; Volatilization; Evaporation; Vadose zone

1. Introduction

Most numerical models of flow and transport through the vadose zone assume that flow is independent of solute concentration. However, the presence of some chemicals in water can affect the physical properties of the fluid phases, and the resulting transport processes are known as non-passive. Thus, modeling of infiltration, redistribution and volatilization/evaporation of these aqueous mixtures should take into account their non-passive transport behavior.

Various authors have already considered the dependence of some properties on concentration. For example, Boufadel et al. [6] developed a one-dimensional model to simulate the density-dependent flow of salt water in variably saturated media. They found that the concentration at the front and the flux front position and magnitude propagate faster in the case of density-dependent solutions than in the case of passive transport. In a later study, Boufadel et al. [7] expanded their model to take into account density-and-viscosity-dependent flow in two-dimensional variably saturated porous media and used it to investigate beach hydraulics at seawater concentration in the context of nutrient delivery for bioremediation of oil spills on beaches. Numerical simulations applied to a rectangular section of a hypothetical beach showed that buoyancy in the

* Corresponding author. Tel.: +34 977 55 96 39; fax +34 977 55 96 21.
E-mail addresses: orlando.silva@urv.cat (O. Silva), jordi.grifoll@urv.cat (J. Grifoll).

0309-1708/$ - see front matter © 2006 Elsevier Ltd. All rights reserved.
doi:10.1016/j.advwatres.2006.06.004

unsaturated zone is significant in anisotropic fine-textured soils with low dispersivities. In all the cases considered, the effects of concentration-dependent viscosity were negligible compared to the effects of concentration-dependent density. Ouyang and Zheng [33] used the model FEMWATER to simulate the transport of two chemicals, one with relatively low water solubility (aldicarb) and the other with relatively high water solubility (acephate), through an unsaturated sandy soil. Comparison of simulations showed that the effects of solution density on the transport of aldicarb were negligible, whereas acephate, with density-driven transport, migrated 22% deeper into the soil in a period of 90 days than without considering density-driven transport. They also performed a numerical experiment including a viscosity–concentration relationship, but the results indicated that the effect of the viscosity was negligible compared with the effect of density for the simulation conditions used in their study. The study of Ouyang and Zheng [33] suggested that under certain circumstances, e.g., high chemical concentration, high water solubility, and high pure chemical density, exclusion of the density-induced mechanism could result in inaccurate predictions of water movement and chemical leaching through the vadose zone. These usual simplifications could also lead to inadequate interaction between the different mass transfer mechanisms when they are included in modeling of transport through reactive soils. As Zhang et al. [48] pointed out, concentrated aqueous solutions are significantly different from dilute solutions in transport and geochemical processes because of their large density, viscosity, and complicated ionic interactions.

A number of studies of the effects induced on the flow by surfactants have emphasized their non-passive transport behavior in the vadose zone. Smith and Gillham [43] developed an isothermal saturated–unsaturated flow and transport model with solute concentration-dependent surface tension. They applied the model to simulate the infiltration of aqueous solutions of butanol and methanol into two soils with different silt contents. Their numerical simulations indicated that solutes that depress surface tension cause a local increase in the hydraulic head gradients, which increases the liquid fluxes and the solute transport. Smith and Gillham [44] complemented their previous work with laboratory experiments conducted in saturated–unsaturated column sand. In this second work, they also incorporated the effect of concentration-dependent viscosity into their earlier model [43] to scale the unsaturated hydraulic conductivity. From their experimental data and numerical simulations, they distinguished two flow effects associated with concentration-dependent surface tension in the vadose zone: (i) the transient unsaturated flow caused by changes in pressure head, and (ii) a decrease in the height of the capillary fringe. Both effects were proportional to the changes in the relative surface tension with solute concentration. They also observed that higher water contents were obtained in steady state for the butanol solution than for water and attributed this difference to the relatively higher viscosity of the butanol solution. Henry et al. [19] studied the effect of solute solubility on unsaturated flow and concluded that the surfactants can significantly affect the flow in unsaturated porous media. Through a series of closed, horizontal sand column experiments, they demonstrated that the surfactant-induced flow caused by a highly soluble compound such as butanol was very different from the flow caused by a relatively insoluble surfactant such as myristyl alcohol, though both induced a similar reduction in the surface tension of water. This difference was attributed to the fact that, unlike butanol, myristyl alcohol is virtually insoluble and primarily resides at the air–water interface rather than in the bulk solution. Thus, flow only occurs at surfactant concentrations that are greater than or equal to those needed to completely cover the air–water interface, which leads to an ineffective transport of myristyl alcohol to previously clean regions [23]. In another study of surfactant-induced flow phenomena, Henry et al. [20] found that hysteresis was an important factor in horizontal flow. They conducted experiments in closed, horizontal columns filled with silica sand and with butanol as the surfactant. They also modified a one-dimensional hysteretic unsaturated flow and transport numerical model to include the dependence of surface tension and viscosity on concentration. Under hysteretic conditions and at final steady state, the model predicted uniform concentration and pressure profiles, but a non-uniform liquid content profile unlike the situation expected if the system was non-hysteretic. Also, flow simulations were sensitive to dispersivity. As Henry et al. [20] noted, lower dispersivity caused sharper surfactant concentration gradients, which led to larger capillary pressure gradients and higher fluxes near the solute front. In the same context, these authors [22] modified a two-dimensional model for flow and transport in unsaturated soils to include the dependence of surface tension and viscosity on the surfactant concentration. They directly compared the simulations to the sand box infiltration experiments with butanol–water mixtures presented by Henry and Smith [21]. A longitudinal dispersivity value of 1 cm was used in the simulations and shown to cause too much dispersion relative to the experimental data at larger travel distances. In a recent review of the surfactant-induced flow phenomena in the vadose zone, Henry and Smith [23] presented experimental evidence that surfactant-induced flow effects can be significant when considered on the laboratory scale. These effects may be due to surfactant modifications of moisture retention characteristics and unsaturated hydraulic conductivity, which affect unsaturated flow and chemical transport. They also recognized that more work is needed to better understand the potential impact of surfactant-induced flow effects on field-scale transport in the vadose zone and suggest that models should include a better description of processes and phenomena such as hysteresis in the hydraulic functions, vapor-phase transport of surfactant or partitioning of surfactant to the different phases.

Despite all of these studies, the effects of several common simplifications for modeling non-passive transport of solutes have still not been evaluated. Although several numerical models can be adapted to simulate some situations of non-passive transport through the vadose zone in multiphase systems, e.g., STOMP [46,47] and VST2D [13], in most of them it is considered that several properties are independent of the mixture composition.

In this paper, we present a model for non-passive infiltration–redistribution and transport of water-soluble solutes in the vadose zone. This model incorporates the dependence of density, viscosity, surface tension, molecular diffusion coefficient in the liquid-phase, and the gas–liquid and solid–liquid partition coefficients, on the solute concentration. We also include the reduction in the gas–liquid partition coefficient due to high capillary pressures in accordance with Kelvin's equation for multicomponent mixtures. The effects of these dependencies were illustrated using a one-dimensional numerical implementation of the transport model to simulate the infiltration, redistribution and volatilization of alcohol–water mixtures into different soils.

2. Basic equations and numerical resolution

2.1. Balance equations

The unsaturated soil system considered consists of liquid (l), gas (g) and solid (s) phases. Components that may be present within these phases are water, dry-air and $N-2$ water-soluble organic compounds. The mass-conservation equations for component k under isothermal conditions were described by [17]

$$\frac{\partial \theta_l C_l^k}{\partial t} = -\nabla \cdot [\boldsymbol{J}_l^k + \boldsymbol{q}_l C_l^k] - a_{lg}^k N_{lg}^k - a_{ls}^k N_{ls}^k \tag{1a}$$

$$\frac{\partial \theta_g C_g^k}{\partial t} = -\nabla \cdot [\boldsymbol{J}_g^k + \boldsymbol{q}_g C_g^k] + a_{lg}^k N_{lg}^k \tag{1b}$$

$$\frac{\partial \theta_s C_s^k}{\partial t} = a_{ls}^k N_{ls}^k \tag{1c}$$

where C_i^k (kg/m^3) is the concentration of component k ($k = 1,\ldots,N$) in the phase i ($i = \mathrm{l,g,s}$), θ_i (m^3/m^3) is the volumetric fraction of that phase, $\boldsymbol{q}_i$ (m/s) is the i phase specific discharge, N_{ij}^k (kg/m^2 s) is the interface mass flux of component k from phase i to phase j, and a_{ij}^k (m^2/m^3) is the interfacial area between phases i and j by unit volume of porous matrix. The diffusive–dispersive mass flux vector $\boldsymbol{J}_i^k$ (kg/m^2 s) is given by

$$\boldsymbol{J}_i^k = -\theta_i \boldsymbol{D}_i^k \nabla C_i^k \tag{2}$$

where $\boldsymbol{D}_i^k$ (m^2/s) is the diffusion–dispersion tensor for component k [4]. Under the assumption of local phase equilibrium [17], the three component equations (1) can be combined to give

$$\frac{\partial \varphi_k C_l^k}{\partial t} = -\nabla \cdot (\boldsymbol{J}_l^k + \boldsymbol{J}_g^k + \boldsymbol{\beta}_k C_l^k) \tag{3a}$$

$$\varphi_k = \theta_l + \theta_g H_{gl}^k + \theta_s H_{sl}^k \tag{3b}$$

$$\boldsymbol{\beta}_k = \boldsymbol{q}_l + \boldsymbol{q}_g H_{gl}^k \tag{3c}$$

Assuming that dry-air is present neither in the liquid-phase nor in the solid-phase, only the gas-phase transport (Eq. (1b)) was considered for the dry-air mass-conservation equation

$$\frac{\partial \theta_g C_g^a}{\partial t} = -\nabla \cdot [\boldsymbol{J}_g^a + \boldsymbol{q}_g C_g^a] \tag{4}$$

where C_g^a is the dry-air concentration in the gas-phase.

The specific discharge of phase i, $\boldsymbol{q}_i$ (m/s), is given by the generalized Darcy's law [4]

$$\boldsymbol{q}_i = -\frac{\boldsymbol{k} k_{ri}}{\mu_i}(\nabla P_i + \rho_i g \boldsymbol{z}) \tag{5}$$

In Eq. (5), $\boldsymbol{k}$ is the intrinsic permeability tensor of the soil (m^2), $g\boldsymbol{z}$ (m/s^2) is the gravity vector, k_{ri} is the relative permeability (dimensionless), ρ_i (kg/m^3) is the density, μ_i (kg/m s) is the dynamic viscosity, and P_i (Pa) is the pressure of phase i.

The diffusive–dispersive mass flux vector of air $\boldsymbol{J}_g^a$ (kg/m^2 s) was calculated from the condition

$$\sum_{k=1}^{N} \boldsymbol{J}_g^k = 0 \tag{6}$$

The partition coefficient, H_{ij}^k, between phases i and j is defined by

$$H_{ij}^k = \frac{C_i^k}{C_j^k}, \quad i,j = \mathrm{g,l,s} \tag{7}$$

Use of constant partition coefficients is a common assumption when modeling solute transport in variably saturated soils. However, in this work the gas–liquid partition coefficient, H_{gl}^k, was assumed to be dependent on solute concentration and soil–liquid content [10–12] as given by

$$H_{gl}^k = H_{gl}^{*k} \exp\left(\frac{P_M \widehat{V}_k}{RT}\right) \tag{8}$$

where the exponential term accounts for the Kelvin's effect in multicomponent liquid mixtures [39,42]. In (8), $\widehat{V}_k$ (m^3/mol) is the partial molar volume of component k in the liquid-phase, R (Pa m^3/K mol) is the universal gas constant, $P_M = P_l - P_g$ (Pa), is the matric pressure of the liquid and T (K) is the temperature. The gas–liquid partition coefficient for plane interfacial surfaces corresponds to the dimensionless Henry's law constant, H_{gl}^{*k}, and its dependence on component concentration was calculated from the liquid–vapor equilibrium condition [45]

$$H_{gl}^{*k} = \gamma_k \frac{p_{vap}^k \widehat{V}_m}{RT} \tag{9}$$

in which p^k_{vap} (Pa) is the vapor pressure of component k, $\widehat{V}_m$ (m^3/mol) is the partial molar volume of the liquid mixture, and γ_k (dimensionless) is the activity coefficient of component k. In very dry soil conditions, the small quantity of liquid in the medium is no longer under the influence of capillary forces so, strictly speaking, the original matric pressure definition is not applicable. Nevertheless, as Baggio et al. [3] suggested, the matric pressure definition can be expanded as

$$P_M = -\frac{\Delta h}{\widehat{V}_m} \tag{10}$$

where Δh (J/mol) refers to the enthalpy difference between the vapor in the gas-phase and the condensed and/or adsorbed liquid-phase, excluding the latent enthalpy of vaporization. Taking this definition, matric pressure and Kelvin's equation can be applied throughout all the range from wet to dry conditions [15,41].

2.2. Boundary conditions, dispersivities and numerical procedure

In this work, the one-dimensional version of the non-passive transport model described previously was implemented to simulate the infiltration, redistribution and volatilization/evaporation of alcohol–water mixtures in soils. A dynamic boundary condition at the surface was set to accommodate either a given infiltration or an evaporation/volatilization flux. In case of infiltration, the top boundary condition for the transport of each component (Eq. (3)) was the component mass flux at the surface, N^k_0 (kg/m^2 s), calculated as

$$N^k_0 = q_{l0} C^k_{l,in} \tag{11}$$

where q_{l0} (m/s) is the given infiltration liquid specific discharge and $C^k_{l,in}$ (kg/m^3) is the concentration of component k in the infiltrating liquid. In the absence of infiltration, the evaporation/volatilization mass flux for component k at the surface was calculated by considering a mass transfer limitation from the soil surface to the bulk atmosphere

$$N^k_0 = k^k_0\left(C^k_{bk} - C^k_{g0}\right) \tag{12}$$

In Eq. (12), k^k_0 (m/s) is the atmosphere-side mass transfer coefficient for component k, C^k_{bk} (kg/m^3) is the background concentration of component k in the atmosphere, and C^k_{g0} (kg/m^3) is the concentration of component k in the gas-phase at the soil surface. For given values of wind velocity, soil roughness and Schmidt number of the volatilized chemical, the mass transfer coefficients, k^k_0, were estimated with the semi-empirical correlation proposed by Brutsaert [8]. This correlation is only applicable under neutral atmospheric conditions and was developed from available experimental data. In case of non-neutral conditions a different approach using the Obukhov length should be used as suggested by Brutsaert [8]. In all cases, the boundary condition at the bottom was set as zero diffusive and dispersive fluxes and zero matric pressure gradient. The lower gas-phase boundary condition was set as a no-flow boundary, while the upper gas-phase boundary condition was a constant atmospheric pressure.

The longitudinal diffusion–dispersion coefficient for component k, D^k_i (m^2/s), was calculated as

$$D^k_i = \frac{D^k_{0i}}{\tau_i} + D_{Li} \tag{13}$$

where the molecular diffusion and the longitudinal dispersion coefficients in phase i are denoted by D^k_{0i} (m^2/s) and D_{Li} (m^2/s), and τ_i (dimensionless) is the tortuosity of phase i. Tortuosities, τ_g and τ_l, were evaluated according to the first model of Millington and Quirk as suggested by Jin and Jury [25], i.e. $\tau_i = \varepsilon^{2/3}/\theta_i$, where ε is porosity. Longitudinal dispersion coefficients for each phase were calculated as $D_{Li} = \alpha_{Li} q_i/\theta_i$, where α_{Li} (m) is the longitudinal dispersivity for phase i given as a function of the volumetric phase content, in accordance with the correlation proposed by Grifoll et al. [18]

$$\alpha_{Li} = \alpha^0_{Li}(13.6 - 16S_i + 3.4S^5_i) \tag{14}$$

in which $S_i = \theta_i/\varepsilon$ is the actual saturation of phase i and α^0_{Li} is the dispersivity at saturation. Grifoll and Cohen [17] used a similar approach to Eq. (14). As they pointed out, the adoption of an empirical longitudinal dispersivity model, like described by Eq. (14), is not meant to suggest its general applicability, but can be used to illustrate a general trend in dispersivity behavior.

The governing partial differential equations, Eqs. (3) and (4), were discretized spatially and temporally in algebraic form using the finite volumes method [34] with a fully implicit scheme (backward Euler) for time integration. The non-linear discretized governing equations were solved using the multivariable Newton–Raphson iteration technique [26]. Volumetric liquid content, dry-air concentration in the gas-phase and alcohol concentration in the liquid-phase were selected as primary variables. The Jacobian coefficient matrix was calculated using a finite difference approximation [26]. The linear system of equations formulated in the Newton–Raphson method was solved for the correction to the primary variables by the iterative Preconditioned Biconjugate Gradient Method [26,35]. The preconditioner matrix was the diagonal part of the Jacobian coefficient matrix [35]. Values for the convergence limit and maximum number of Newton–Raphson iterations have been defined conveniently as input parameters. Convergence limits were defined with respect to the maximum residual of each mass balance equation, normalized by the sum of the mass fluxes absolute values. The tolerance employed in all simulations was 10^{-7} while the maximum number of Newton–Raphson iterations was set to 10. If the convergence limit was not satisfied after 10 iterations, the time step was reduced to 50% and the calculation was restarted from the end of the previous time step. Otherwise, if the convergence was attained within the maximum number of iterations, the time step was doubled without

exceeding a maximum $\Delta t_{max} = 60$ s, and a new time step was initiated.

The one-dimensional grid was generated by distinguishing two regions. First, from the surface to a depth of $z = 0.135$ m and starting with $\Delta z_1 = 0.2$ mm, the grid spacing increases with a progression factor of 1.008. Second, from $z = 0.135$ m to the bottom of the system ($z = 0.5$ m) the grid was set uniform with a grid spacing of $\Delta z = 1.33$ mm.

The sensitivity of the numerical solution to grid spacing and time step was analyzed for Test Case I as it is described in Section 3.2.1 below. For the standard grid and maximum time step given above, maximum discrepancies between the numerical results and the exact values are expected to be less than 1%.

To check the numerical algorithm, we compared the solution of the passive transport of water–methanol mixtures into a loam-type soil with the solution reported by Grifoll and Cohen [17]. The maximum discrepancy between these two solutions was also less than 1%.

3. Results and discussion

The present numerical model has been used to simulate several test cases in order to investigate the non-passive transport behavior of volatile organic compounds. The first test presented is the infiltration of water–butanol mixtures into sand as reported by Smith and Gillham [44]. Their experimental and simulation results were compared to the present numerical results in order to check our model, the numerical algorithm and the computational code. The next two test cases were for the infiltration of methanol–water mixtures into a sandy clay loam and silty clay soils. These test cases illustrated how the dependency of physical properties on concentration affects a system in which the solute is soluble in water at any proportion. Initial test simulations showed that the convective gas-phase component did not contribute effectively to the transport of methanol and water. In the present test cases of soils with relatively low permeabilities, the inclusion of gas-phase convection did not change the evolution of the volumetric liquid content and methanol concentration profiles by more than 0.5% and very high CPU times were required. Note that the differences in gas-phase densities due to the saturation or absence of methanol were not high enough to induce density-dependent advection [28]. In addition, as stated by Lenhard et al. [28], effects of density-driven vapor flow are more evident in porous media with permeabilities grater than 10^{-11} m^2. On the contrary, the permeabilities of the soils studied in this work are less than 4×10^{-13} m^2. Most of the results presented in the next sections were therefore obtained by neglecting gas-phase convection when solving the numerical model.

3.1. Dissolved butanol infiltration

Smith and Gillham [44] studied the infiltration of a butanol–water mixture into a 2 m column sand. Their experimental procedure consisted of infiltrating distilled water until the steady state was reached and then changing the infiltration liquid to an aqueous solution of butanol with 7% w/w at the same infiltration rate. Their experimental results were compared with their earlier numerical transport model [43], which was modified to include the dependencies of surface tension and viscosity on butanol concentration. Fig. 1 shows the evolution of the pressure head and liquid content measured at a depth of 38 cm in the column, the simulation results of Smith and Gillham [44], and the present numerical calculations. For the present simulation, the dependency of surface tension and viscosity on solute concentration, as well as the soil water retention curve, were taken from Smith and Gillham [44]. A measured constant dispersivity $\alpha_{Li} = 0.00177$ m [44] was also used in this case.

Deviations from steady state in pressure head and liquid content after the application of butanol solution were observed. These variations were due to the dependency of surface tension and viscosity on butanol concentration.

As the solute front passed, the water content significantly decreased to a minimum before increasing to a slightly higher value than that of the previous steady state. The highly localized drainage and rewetting were caused by hydraulic gradients induced by the surface tension variations associated with the solute front.

Both the model of Smith and Gillham [44] and the present model describe the main characteristics of the experiment. It should be noted that the model parameters used by Smith and Gillham [44] were estimated independently of the experimental results that appear in Fig. 1. They suggested that some experimental uncertainty could be introduced in the measurement of dispersivity because it was determined using a concentrated solution of NaCl that could be subject to density effects. Moreover, the differences in the pressure head and volumetric liquid content between the two simulation results were less than 4.8%,

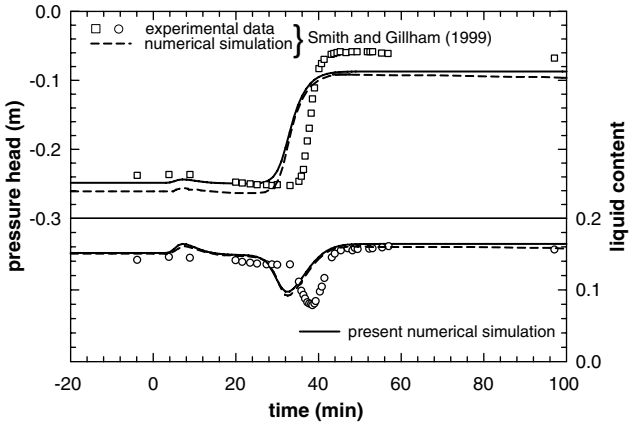

Fig. 1. Evolution in time of pressure head and liquid content at 38 cm depth for the infiltration in sand of a water–butanol solution at 7% w/w. Comparison of experimental and numerical simulation data of Smith and Gillham [44] with present numerical simulation.

which gives an indication of the ability of the present model to simulate non-passive transport of solutes.

3.2. Methanol infiltration

The impact of the non-passive behavior on the infiltration and redistribution of methanol–water mixtures is illustrated in two cases in which different soils were used. In both of these test cases we simulated a hypothetical scenario composed by an initial period of infiltration followed by a period of volatilization/evaporation. Therefore, at least close to the soil surface where volatilization and evaporation occur, the soil was expected to reach conditions of very low liquid content ($\theta_l < 0.10$). To simulate these situations realistically, we used an extended version of the Brooks–Corey soil–water retention curve proposed by Rossi and Nimmo [38], which is given as

$$P_{M,w}(S) = \begin{cases} P_d e^{-S/\alpha_{RN}} & 0 \leqslant S < S_j \\ P_b S_e^{-1/\lambda} & S_j \leqslant S \leqslant 1 \end{cases} \quad (15)$$

In Eq. (15) $S = \theta_l/\varepsilon$ and $S_e = (S - S_r)/(1 - S_r)$ are the actual and effective liquid saturation, respectively, $P_{M,w}$ (Pa) is the matric water pressure, while P_b (Pa) (bubble pressure or air entry pressure), λ (pore size distribution index), and θ_r (residual volumetric water content) are the classical Brooks–Corey parameters. The oven dry matric water pressure, P_d, was taken as 980 MPa, as suggested by Rossi and Nimmo [38]. The parameters α_{RN} and θ_j ($S_j = \theta_j/\varepsilon$), introduced by these authors, were calculated as functions of the classical Brooks–Corey parameters, as suggested by Morel-Seytoux and Nimmo [31]. Liquid-phase relative permeability was computed as a function of liquid saturation from the soil-moisture retention function according to the model of Burdine [9]

$$k_{rl} = S^2 \frac{I(S)}{I(1)} \quad (16)$$

where

$$I(S) = \begin{cases} \frac{\alpha_{RN}}{2P_d^2}(e^{2S/\alpha_{RN}} - 1) & 0 \leqslant S < S_j \\ \frac{\alpha_{RN}}{2P_d^2}(e^{2S_j/\alpha_{RN}} - 1) + \frac{\lambda}{\lambda+2}\frac{(1-S_r)}{P_b^2}(S_e^{1+2/\lambda} - S_{ej}^{1+2/\lambda}) & S_j \leqslant S \leqslant 1 \end{cases} \quad (17)$$

Given a volumetric liquid content, the matric pressure for pure water as given by Eq. (15) has been scaled for mixtures with the methanol concentration C_l as [29]

$$P_M = \frac{\sigma(C_l)}{\sigma_w} P_{M,w} \quad (18)$$

where σ_w is the surface tension of water and $\sigma(C_l)$ (N/m) is the surface tension of the liquid mixture.

The physical properties of methanol–water mixtures depend on methanol concentration. In this work, each of these dependencies has been described by a polynomial function, as

$$p(C_l) = \sum_j a_j (C_l)^j \quad (19)$$

where p stands for any of the properties allowed to vary with methanol concentration (surface tension, density, viscosity and diffusion coefficient of methanol in the liquid-phase) and C_l is the methanol concentration in the liquid-phase. The polynomial coefficients a_j, obtained by fitting Eq. (19) to available experimental data [14], are given in Table 1. Diffusion coefficients of methanol and water in the gas-phase were taken as constants, with values $D_{0g}^m = 1.6 \times 10^{-5}$ m^2/s [17] and $D_{0g}^w = 2.6 \times 10^{-5}$ m^2/s [37], respectively.

To calculate the gas–liquid partition coefficients for methanol and water, the partial molar volumes and the activity coefficients according to Eqs. (8) and (9) are required. Activity coefficients for water and methanol were calculated using Wilson's equation [27] with the parameters fitted by Gmehling et al. [16] to available experimental data. Molar volumes were calculated following the procedure described by Lide and Kihiaian [30], who suggested the Redlich–Kister equation to calculate molar excess volumes. The gas–liquid partition coefficients H_{gl}^* for water and methanol calculated by this procedure are shown in Fig. 2. For water, this partition coefficient increases monotonically from 1.73×10^{-5}, in absence of methanol, to the limiting value 6.14×10^{-5} as the pure methanol condition is approached. The partition coefficient for methanol reaches a minimum value of 1.61×10^{-4} when $C_l = 405$ kg/m^3 and then increases progressively to 2.17×10^{-4}, which is the value for pure methanol. Sorption of methanol onto the soil solid was assumed to be described by a constant partition coefficient $H_{sl}^m = 3.7 \times 10^{-3}$, estimated for a soil with 2% of organic matter [17]. In their experimental work, Smith and Gillham [44] used homogeneous sand and therefore found low values of dispersivity. In heterogeneous natural soils higher dispersivities are expected. Jaynes [24], for instance, obtained values of dispersivity between 0.0453 and 0.25 m for a depth of 0.3 m. Also,

Table 1
Polynomial coefficients obtained by fit of experimental data[a] at 20 °C to Eq. (19)

Property	a_0	a_1	a_2	a_3	a_4	R^2
σ_l (N m^{-1})	7.275×10^{-2}	-2.134×10^{-4}	5.352×10^{-7}	-6.831×10^{-10}	3.105×10^{-13}	0.996
ρ_l (kg m^{-3})	9.9701×10^{2}	-1.917×10^{-1}	1.665×10^{-4}	-3.340×10^{-7}	–	0.99994
μ_l (kg m^{-1} s^{-1})	1.003×10^{-3}	3.134×10^{-6}	3.710×10^{-9}	-2.082×10^{-11}	1.298×10^{-14}	0.998
D_{0l}^m (m^2 s^{-1})	1.350×10^{-9}	-7.419×10^{-13}	-4.789×10^{-15}	8.486×10^{-18}	–	0.983

[a] Experimental data extracted from Gammon et al. [14].

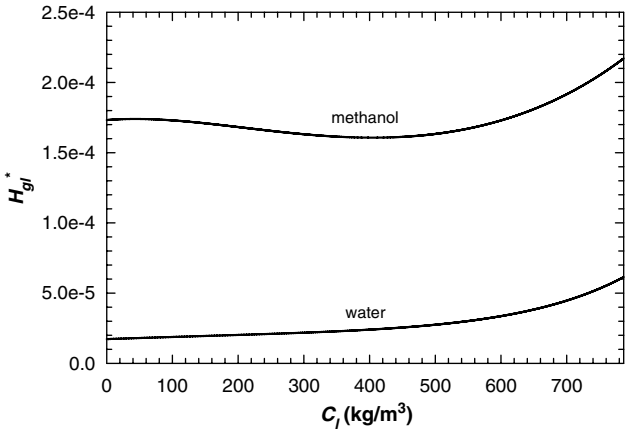

Fig. 2. Gas–liquid partition coefficients for methanol–water system.

Abbasi et al. [1] estimated soil hydraulic and solute transport parameters from several two-dimensional furrow irrigation experiments and obtained values of longitudinal dispersivity between 0.026 and 0.328 m for a depth of 1 m. In this paper, dispersivity at saturation for both the liquid and the gas phases was set to $\alpha_{Li}^0 = 0.078$ m, the value suggested by Biggar and Nielsen [5] for saturated soil conditions in an agricultural field [32]. In their work, Biggar and Nielsen measured dispersivities in ponded soils (of a broad textural class: loam, clay loam, silty clay, silty clay loam) under steady state infiltration conditions at depths between 30.5 and 182.9 cm, infiltration pore velocities between 1.3 and 105.4 cm/day, while hydraulic conductivities at saturation ranged from 0.3 to 70 cm/day. In the test cases of the present work, the selected soils and process conditions were, most of the time, within the range of values above described.

3.2.1. Test case I

The first case study involved five simulations of the infiltration of methanol–water mixtures into a homogeneous sandy clay loam soil, each with different methanol concentration of the infiltrating liquid, $C_{l,in}$. These concentrations ranged from $C_{l,in} = 0.001$ kg/m^3, in which the methanol behaves as a passive scalar, to $C_{l,in} = 786.6$ kg/m^3, which corresponds to pure methanol. The upper boundary condition was set at an infiltration rate of 0.25 cm/h for 15 h, followed by 57 h in which the methanol and water were allowed to volatilize at the surface according to Eq. (12). The background concentration of methanol in the atmosphere was assumed to be zero, while the background concentration of water in the atmosphere was calculated assuming a relative humidity of 40%. The initial condition was a uniform volumetric water content of 0.128 m^3/m^3, which corresponds to a matric potential of −100 m. The hydraulic parameters of Eqs. (15)–(17), taken from Rawls and Brakensiek [36] as typical values for a sandy clay loam soil, are given in Table 2.

When comparing the results of the simulations for different grid spacing and time steps, it is observed that methanol concentration and volumetric liquid content values at the surface are the most sensitive to these variations. Five simulations with different grid spacing were run for a maximum time step of $\Delta t_{max} = 60$ s and $C_{l,in} = 400$ kg/m^3. A coarse grid with $N = 125$ control volumes was used in the first simulation. In the following ones, the number of control volumes N was successively doubled by halving the grid spacing. The methanol concentration and the volumetric liquid content at the surface at the end of the simulations were extrapolated to an infinite number of volumes, C_{l0}^{∞} and θ_{l0}^{∞}. Fig. 3(a) shows the ratio of C_{l0} and θ_{l0} to their extrapolated value C_{l0}^{∞} and θ_{l0}^{∞} as a function of the inverse of the number of control volumes. Deviations from the extrapolated value were higher in the case of methanol concentration. However, for both concentration and volumetric liquid content, and for all grids tested, the relative deviations were less than 0.6%. The sensitivity of simulations to time step was tested using the grid described at the end of Section 2.2 (500 volumes) and $C_{l,in} = 400$ kg/m^3. Five simulations were run with $\Delta t_{max} = 240$, 120, 60, 30 and 15 s and the values at the surface extrapolated to zero time step. Fig. 3(b) shows that methanol concentration at the surface was sensitive to time step, although for $\Delta t_{max} < 240$ s, the concentration differences respect the extrapolated value were less than 5%. For the standard simulation conditions ($N = 500$, $\Delta t_{max} = 60$ s), the maximum deviations expected are less than 1%.

Fig. 4 shows the volumetric liquid content and normalized concentration profiles 48 h after the beginning of the experiment for five methanol concentrations in the

Table 2
Simulation conditions and hydraulic soil properties

	Test case I	Test case II
Simulation conditions		
Soil type	Sandy clay loam	Silty clay
Soil depth (m)	0.5	0.5
Initial pressure head (m), P_{ini}	−100	−500
Infiltration rate (cm/h), q_{l0}	0.25	0.075
Total time of simulation (h)	72	168
Initial period of infiltration (h)	15	20
Dispersivity at saturation (cm), α_{Li}^0	0.2; 7.8	7.8
Atmosphere-side mass transfer coefficient for methanol[a] (kg/m^2 s), k_0^m	3.5×10^{-3}	3.5×10^{-3}
Atmosphere-side mass transfer coefficient for water[a] (kg/m^2 s), k_0^w	4.0×10^{-3}	4.0×10^{-3}
Hydraulic soil properties		
Soil porosity,[b] ε	0.33	0.423
Residual water content,[b] θ_r	0.068	0.056
Brooks–Corey parameter,[b] λ	0.25	0.127
Bubble pressure,[b] P_{bw} (Pa)	2754	3352
Hydraulic saturated conductivity,[b] K_s (cm/h)	0.43	0.09
Volumetric liquid content at junction,[c] θ_j	0.1415	0.3079
Rossi–Nimmo parameter,[c] α_{RN}	0.0557	0.0756

[a] Calculated according to Brutsaert [8] assuming a wind velocity of 2 m/s and a surface roughness length of 1 cm.
[b] From Rawls and Brakensiek [36].
[c] Calculated according to Morel-Seytoux and Nimmo [31].

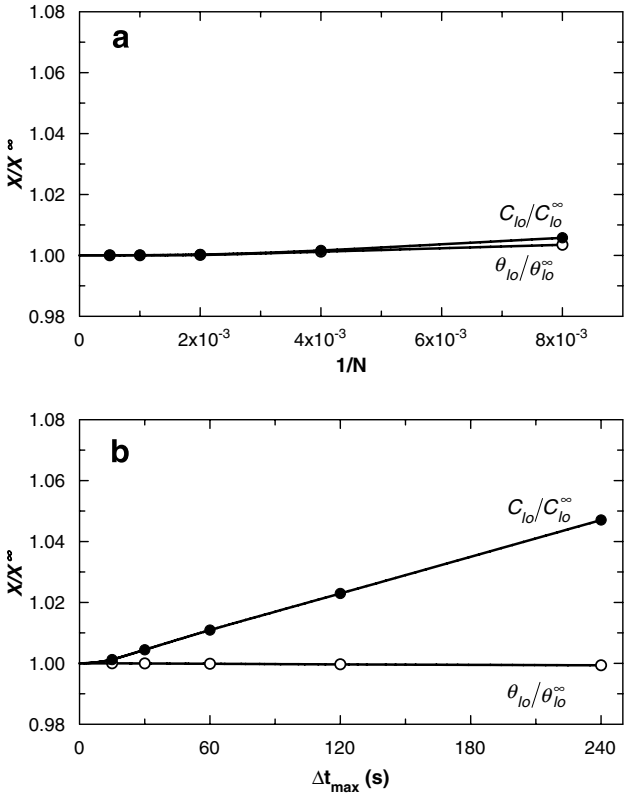

Fig. 3. Dependency of the concentration and liquid content at surface on (a) the grid spacing and (b) the maximum time step.

infiltrating liquid. Normalization has been carried out with respect $C_{l,in}$ in order to emphasize the non-passive behavior because, in the case of passive transport, the normalized concentration profiles in Fig. 4 should be independent of concentration since the solute transport equation (3) is linear when the coefficients do not depend on the solute concentration.

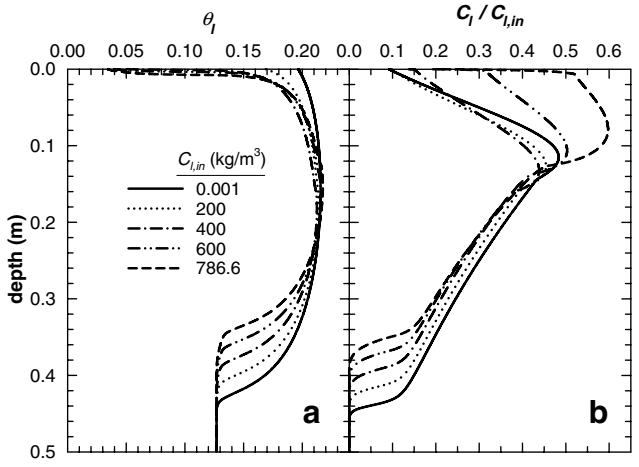

Fig. 4. Infiltration and redistribution of methanol–water mixtures of different compositions into a sandy clay loam soil. Simulation results after 48 h and a dispersivity of 7.8 cm. (a) Volumetric liquid content, (b) methanol concentration in the liquid-phase.

The differences in volumetric liquid content profiles for different $C_{l,in}$, shown in Fig. 4(a), are due to three factors: (i) the dilution effect on the incoming mixture caused by the initial pure water in the soil, (ii) differences in the liquid-phase flow caused by changes in viscosity, density and surface tension, and (iii) the volatilization of the mixture. Note that the relative densities of the mixture change from 1 for pure water to 0.786 for pure methanol. Then, when methanol dilutes in water, the volume of the mixture should shrink due to the non-ideal mixing effects as described by the dependence of density on concentrations (Eq. (19) and Table 1). This effect is more pronounced when the infiltrating mixture is more concentrated in methanol. During infiltration the causes of the differences in volumetric liquid content are this non-ideal mixing effect and the changes in liquid flow caused by variations in viscosity and surface tension. In the case of pure methanol and after 48 h of simulation (i.e. 33 h of volatilization), by balancing the volumes of initial water, infiltrated liquid, final liquid in the soil and volatilized liquid, it was calculated that the non-ideal mixing effect is about 3.6% of the initial water plus infiltrated liquid volume, whereas the percentage of volatilized liquid is about 9.6%. The relative influence of changes in liquid flow due to variations in viscosity and surface tension cannot be deduced from this balance, but the percentage of volatilized liquid increases from 5% of the initial plus infiltrated volume for pure water, to a maximum of 10% at a concentration of $C_{l,in} = 400$ kg/m^3, and then decreases to 9.6% for pure methanol. Note that the viscosity of the liquid is a concave function of the methanol concentration, reaching a maximum at about 392 kg/m^3. This shows that more viscous infiltrating mixtures move more slowly and consequently, by remaining close to the surface for a longer period, undergo a higher volatilization. Because of the combined effect of volatilization, viscosity and surface tension dependent flow, and non-ideal mixing, the front position for passive transport ($C_{l,in} = 0.001$ kg/m^3) is 29.4% deeper than for pure methanol ($z = 0.34$ m). Moreover, the liquid content near the surface also depends on $C_{l,in}$ because, as is explained below, the volatilization rate at the surface is low for low concentrations of methanol.

The gas–liquid partition coefficient for methanol is between 6 and 10 times higher than for water (see Fig. 2). Higher overall volatilization rates are therefore observed for more concentrated mixtures. The differences in the normalized methanol concentration profiles developed at the soil top (Fig. 4(b)) are largely due to methanol transfer limitations from inside the soil to the surface, which are higher for more dilute mixtures. This is shown in Fig. 4(b), where we find progressively larger differences between the concentration profiles established in the first 10 cm adjacent to the soil surface, especially for $C_{l,in} > 400$ kg/m^3.

The volatilization flux of methanol N_0^m, normalized by the corresponding flux at the beginning of volatilization $N_{0,ini}^m$, is shown in Fig. 5(a) for the five numerical experiments. Volatilization decreases as the methanol concentration and liquid content at surface decrease. These

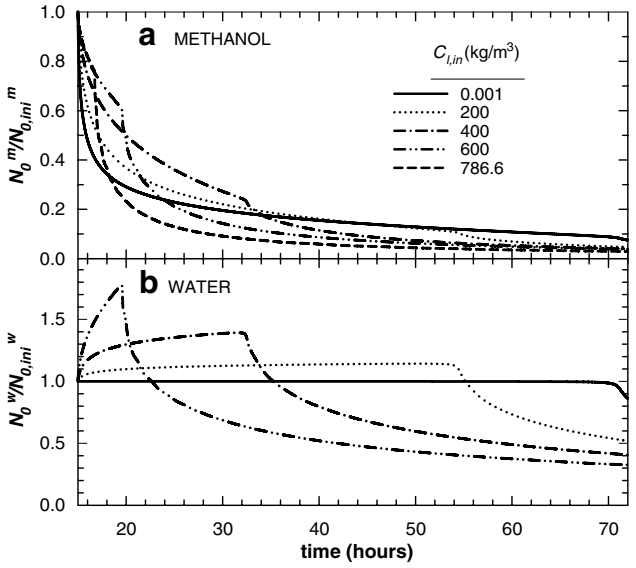

Fig. 5. Evolution of normalized methanol volatilization and water evaporation fluxes for several infiltration methanol concentrations. (a) Volatilization of methanol, (b) evaporation of water.

volatilization fluxes suffer a sudden decrease due to the development of high capillary pressures near the surface, which reduce the gas–liquid partition coefficient according to the exponential term in Eq. (8) (Kelvin effect). This behavior is similar to the decrease in soil water evaporation rates from stage-one to stage-two evaporation [40]. At high infiltration methanol concentrations, volatilization rates are higher. This leads sooner to these high capillary pressures and, therefore, to the observed decrease in the volatilization flux.

The evaporation flux of water N_0^{w} undergoes a similar sudden regime change. However, as shown in Fig. 5(b), after the infiltration has ceased the water evaporation rate increases due to the loss of methanol to the atmosphere, which increases the concentration of water at the soil surface. This initial period of increasing evaporation lasts until Kelvin's effect begins to be noticeable. During this first stage, normalized evaporation is higher at higher infiltrating methanol concentrations. Similar behavior in the time variation of the evaporation flux of water was experimentally and numerically observed by Chen et al. [11]. It is worth noting that when the Kelvin equation and the water vapor diffusion were not included in their water transport model, the simulation results deviated from the experimental measurements.

The role of the various contributions to total liquid movement can be illustrated by inspecting the individual partial fluxes due to capillary component and gravitational component. The partial fluxes can be defined, according to Eq. (5), as given below

$$q_{\mathrm{l,cap}} = -\frac{kk_{\mathrm{rl}}}{\mu_{\mathrm{l}}}\frac{\partial P_{\mathrm{l}}}{\partial z} \tag{20a}$$

$$q_{\mathrm{l,grav}} = \frac{kk_{\mathrm{rl}}}{\mu_{\mathrm{l}}}\rho_{\mathrm{l}} g \tag{20b}$$

where $q_{\mathrm{l,cap}}$ and $q_{\mathrm{l,grav}}$ are the capillary and gravitational components of the flux, respectively.

The contribution made by each of these components to the specific discharge after 48 h of simulation and for each infiltration concentration is shown in Fig. 6. For all cases, the contribution from the gravity flux was negligible and the main contribution was from capillary flux. There were significant differences in the capillary liquid flux due to the relative differences in dryness at the surface and the different viscosity profiles from different compositions of the infiltrating methanol–water mixture. Note that, for $C_{\mathrm{l,in}} \geqslant 400$ kg/m^3 and close to the surface, the liquid flux drops to almost zero because of the low liquid content in this zone (see Fig. 4(a)), which makes the relative permeability negligible. On the other hand, the matric pressure depends on both the liquid content and the solute concentration. We can therefore divide the capillary flux into two components—one that is due to changes in volumetric liquid content and one to changes in the composition of the liquid mixture. These components are defined as

$$q^{C}_{\mathrm{l,cap}} = -\frac{kk_{\mathrm{rl}}}{\mu_{\mathrm{l}}}\frac{\partial P_{\mathrm{l}}}{\partial C_{\mathrm{l}}}\frac{\partial C_{\mathrm{l}}}{\partial z} \tag{21a}$$

$$q^{\theta}_{\mathrm{l,cap}} = -\frac{kk_{\mathrm{rl}}}{\mu_{\mathrm{l}}}\frac{\partial P_{\mathrm{l}}}{\partial \theta_{\mathrm{l}}}\frac{\partial \theta_{\mathrm{l}}}{\partial z} \tag{21b}$$

where $q^{C}_{\mathrm{l,cap}}$ is the capillary liquid flux due to changes in methanol concentration and $q^{\theta}_{\mathrm{l,cap}}$ is the corresponding flux due to variations in the liquid content. Fig. 7 shows the contributions of these components for $C_{\mathrm{l,in}} = 400$ kg/m^3 after 48 h of simulation. We can see that $q^{\theta}_{\mathrm{l,cap}}$ is the main component of the capillary flux and that there is a small contribution of $q^{C}_{\mathrm{l,cap}}$ from $z = 0.15$ m to the front position. Similar contribution profiles were obtained for the other $C_{\mathrm{l,in}}$ cases, which indicates that, in the cases we studied, the main flow mechanism for the infiltration of methanol was the capillary component due to variations in liquid content.

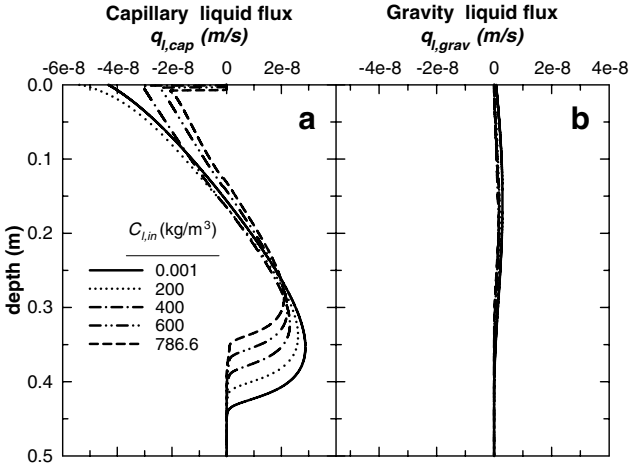

Fig. 6. Liquid flux as function of methanol concentration decomposed into capillary and gravity components, after 48 h of simulation. (a) Capillary liquid flux component, (b) gravity liquid flux component.

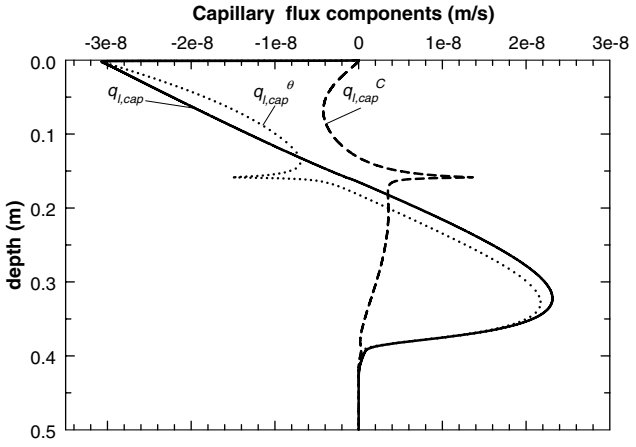

Fig. 7. Capillary liquid flux and its components after 48 h of simulation, $C_{l,in} = 400$ kg/m^3 and a dispersivity of 7.8 cm.

The relative magnitude of the various mechanisms involved in the component transport through the soil can be illustrated by inspecting the individual partial fluxes due to diffusion, dispersion and convection. These partial fluxes are defined for each phase $i = l, g$ and each component k as

$$J^k_{\mathrm{dif},i} = -\theta_i \frac{D^k_{0i}}{\tau_i} \frac{\partial C^k_i}{\partial z} \tag{22a}$$

$$J^k_{\mathrm{disp},i} = -\theta_i D_{\mathrm{L}i} \frac{\partial C^k_i}{\partial z} \tag{22b}$$

$$J^k_{\mathrm{conv},i} = q_i C^k_i \tag{22c}$$

Methanol and water transport by diffusion in the liquid-phase was negligible in all cases. Fig. 8 shows the partial fluxes profiles for methanol and all the relevant mechanisms after 48 h of simulation since the start of the numerical experiment. These mechanisms are diffusion in the gas-phase, $J^{\mathrm{m}}_{\mathrm{dif,g}}$, and dispersion, $J^{\mathrm{m}}_{\mathrm{disp,l}}$, and convection, $J^{\mathrm{m}}_{\mathrm{conv,l}}$, in the liquid-phase. All the fluxes were normalized with respect to the volatilization flux at that time, N^{m}_0. Diffusion in the gas-phase is not an active mechanism for methanol transport, as we can see in Fig. 8(a), except very close to the surface and when $C_{l,in} \geqslant 400$ kg/m^3. In these circumstances the soil close to the surface is very dry (see Fig. 4(a)) and in this region no mechanism in the liquid-phase is able to transport the methanol. Diffusion in the gas-phase is therefore the only active mechanism in this thin region. The methanol concentration gradient that drives the gas-phase diffusion is magnified by the Kelvin effect that decreases the concentration of methanol close to the surface, as the soil becomes drier. Numerical experiments with higher $C_{l,in}$ causes a decrease in the liquid saturation which induce higher gas-phase diffusive fluxes. For $C_{l,in} < 400$ kg/m^3, the top soil is not so dry because volatilization is lower for lower concentrations of methanol. For these low input concentrations, therefore, dispersion in the liquid-phase (see Fig. 8(b)) is the most active mechanism, and accounts for 90% of the transport at the surface.

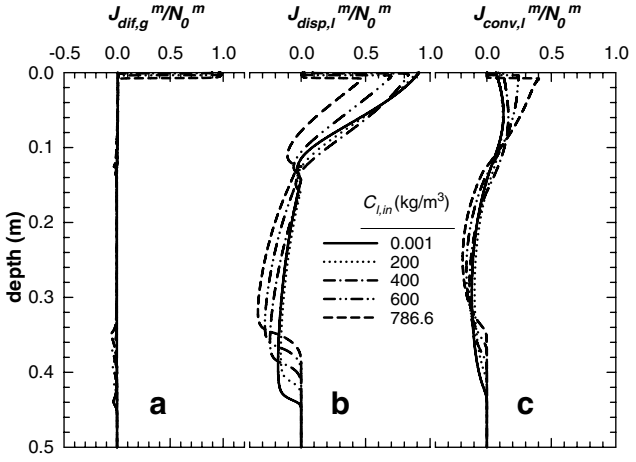

Fig. 8. Normalized partial fluxes in a sandy clay loam soil after 48 h. (a) Diffusive partial flux of methanol in the gas-phase, (b) dispersive partial flux of methanol in the liquid-phase, (c) convective partial flux of methanol in the liquid-phase.

It is important to note the close relationship between the volumetric liquid content and concentration profiles in Fig. 4, the liquid-phase velocities in Fig. 6 and the partial mass fluxes in Fig. 8. For example, at the depth corresponding to the liquid front position for the various cases viscosity increases as the infiltrating mixture becomes more concentrated. As the viscosity is higher, the velocities are lower and a decrease in dispersion in the liquid-phase could be expected. However, the higher the infiltrating concentration, the lower the liquid volumetric content and the higher the methanol concentration gradients. This leads to higher partial dispersive fluxes (Eq. (22b)) in this zone for more concentrated infiltrating mixtures (see Fig. 8(b)). A similar analysis explains the interaction between the liquid-phase velocity, the different transport mechanisms and the liquid content and concentration profiles in the upper part of the soil ($z \leqslant 0.15$ m).

Results of the simulations previously described appear to be inconsistent with experimental and modeling observations of Smith and Gillham [44]. Unlike our simulations that predict a main flow mechanism driven by the capillary component due to variations in liquid content (see Fig. 7), Smith and Gillham [44] observed a significant impact of the solute concentration on unsaturated flow. This discrepancy in principle may be due to our use of a large dispersivity value that reduces the concentration gradient and thereby reduces the magnitude of the effect of the solute on unsaturated liquid fluxes. However, it should be noted that the increase in the matric pressure due to the reduction of the surface tension in accordance with the scaling proposed by Leverett [29] is more pronounced in case of butanol aqueous solution than with aqueous mixtures of methanol. As explained by Smith and Gillham [43] "*butanol, 0–7% by weight at 25 °C, causes a non-linear and relatively large change in surface tension with concentration. Methanol, 0–7% by weight at 25 °C, causes a near linear and relatively*

UNIVERSITAT ROVIRA I VIRGILI
TRANSPORTE NO PASIVO DE COMPUESTOS ORGÁNICOS VOLÁTILES EN LA ZONA NO SATURADA.
Orlando Silva Rojas
ISBN: 978-84-690-7612-5 / DL: T.1217-2007

small change in surface tension". A simple calculus shows that in the case of butanol the reduction is about 70% in the range of 0–7% by weight. Here it is noteworthy that experiments and simulations carried out by Smith and Gillham [43,44] involve scenarios of pure infiltration, unlike our simulations, which include infiltration followed by the volatilization of the mixture. For aqueous solutions of methanol and in the full range of solubility the reduction in surface tension is also 70%. Nevertheless, during volatilization and $C_{l,in} = 400$ kg/m^3, the concentration of methanol within the soil is reduced to less than 40% of this inlet composition, which involves a surface tension reduction of 32%. In order to demonstrate the sensitivity of the results to dispersion, the Test Case I simulations were repeated with a dispersivity value of 0.2 cm. As shown in Fig. 9, the variability in concentration profiles diminished compared to the 7.8 cm dispersivity results, while the differences in volumetric content near the top prevailed due to volatilization. As expected, with a dispersivity of 0.2 cm the solute front is not so dispersed as with 7.8 cm (Fig. 9(b)). Indeed, for a dispersivity of 0.2 cm the solute front is located at a depth that is the half of the liquid front position. An additional observation is that the volumetric liquid content shows a notch just in the solute-front position. This notch was not so evident for a dispersivity of 7.8 cm (Fig. 4(a)), but with a dispersivity of 0.2 cm it grows, especially for the more concentrated mixtures. A similar notch was observed by Allred and Brown [2] in their experiments who concluded that it is caused by a modification in the soil–water retention relationship in the transition zone of the soil between high and low concentrations. Fig. 10 shows the capillary liquid flux and its components for a dispersivity value of 0.2 cm. We can see that now, for $C_{l,in} = 400$ kg/m^3 and at $t = 48$ h (during volatilization), the capillary liquid flux due to changes in the composition is the predominant mechanism

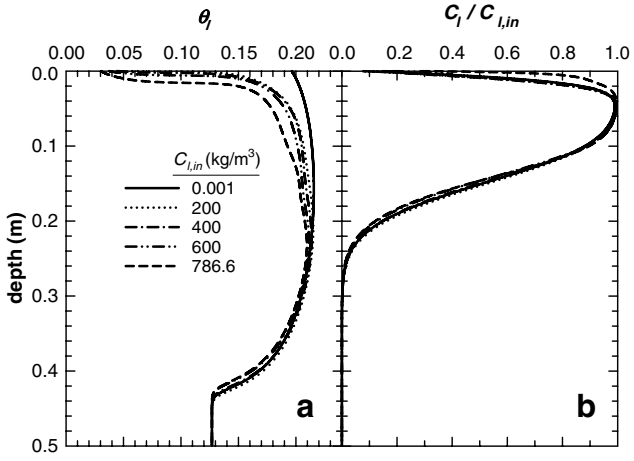

Fig. 9. Infiltration and redistribution of methanol–water mixtures of different compositions into a sandy clay loam soil. Simulation results after 48 h and a dispersivity of 0.2 cm. (a) Volumetric liquid content, (b) methanol concentration in the liquid-phase.

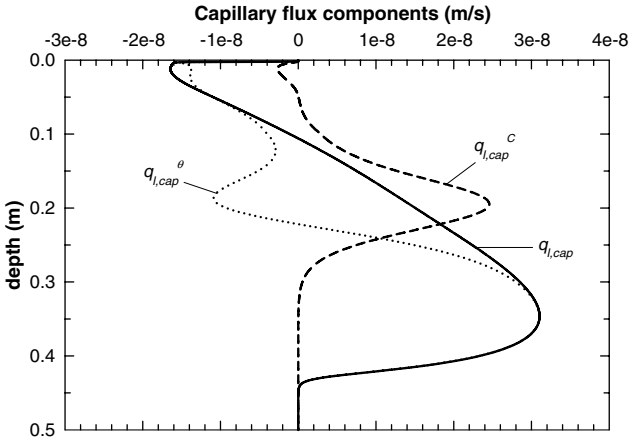

Fig. 10. Capillary liquid flux and its components after 48 h of simulation, $C_{l,in} = 400$ kg/m^3 and a dispersivity of 0.2 cm.

of liquid flow in the region delimiting the solute front. The sensibility analysis of the model to dispersion demonstrates that, for aqueous mixtures of methanol and low dispersivities, changes in surface tension due to variation in composition may induce important liquid flow. This result agrees with simulations and experimental results obtained by other authors [20–22,44].

The coupled non-passive transport of liquid and a solute through the unsaturated zone is therefore a highly interactive phenomenon in which matric pressure gradients can induce solute transport and, reciprocally, mixture composition may change the transport properties and induce a flow pattern.

3.2.2. Test case II

A second case study was carried out to illustrate the potential impact of the Kelvin effect on non-passive transport of solute in the vadose zone and its impact on the volatilization of methanol and the evaporation of water. In some simulations in this case study, the Kelvin exponential factor of Eq. (8) was not considered except at the surface, and the results were compared to simulations in which full consideration of this factor along the system was taken into account. Note that, if the methanol–water mixture is allowed to volatilize/evaporate at a rate that is independent of the liquid content at surface, i.e. ignoring the Kelvin factor, no decrease in volatilization/evaporation fluxes would be observed and a regime like stage-two evaporation [40] would not be attained. With a stage-one like volatilization/evaporation remaining indefinitely, the system would progress to a non-feasible physical situation in which there would be no mechanism for the transport of components from the inside to the soil surface able to maintain these relatively high volatilization/evaporation fluxes dictated by the atmosphere-side mass transfer limitations. In all present simulations, therefore, the Kelvin effect at the surface was considered in order to attain feasible physical situations.

The simulations for this second case were the infiltration and redistribution of a methanol–water mixture into a silty clay soil. The infiltrating methanol concentration was $C_{l,in} = 400\ kg/m^3$ and the infiltration rate was set at 0.075 cm/h for 20 h, followed by 148 h in which the methanol and water were allowed to redistribute and volatilize. Like in the Test Case I we assumed the background concentration of methanol to be zero, and calculated the background concentration of water in the atmosphere assuming a relative humidity of 40%. The hydraulic parameters of a typical silty clay soil were selected as given by Rawls and Brakensiek [36] and listed in Table 2. The hydraulic characteristic of this soil allows high capillary pressures to develop at a relatively high liquid content, a condition for which we expect the Kelvin effect to have a greater impact. The initial condition for the simulation was a constant volumetric water content of $0.169\ m^3/m^3$, which corresponds to a matric head of -500 m.

Fig. 11 shows the liquid content and normalized concentration profiles 48 and 168 h after the start of the simulation (28 and 148 h of volatilization/evaporation, respectively). The dotted line represents the results obtained when the Kelvin effect within the soil is ignored. At both 48 and 168 h, and along the first 5 cm, the volumetric liquid content is lower when the Kelvin factor is allowed to act within the soil. As Fig. 11(a) shows, this difference increases with time as the soil dries. The maximum difference in the volumetric liquid content is located within the first 5 cm adjacent to the soil surface, increasing from 122% after 48 h to 130% after 168 h. For the normalized methanol concentration this difference increases from 33% after 48 h to 43% after 168 h.

To evaluate the impact of including the Kelvin effect in simulations, it is important to note that the main transport mechanism affected is diffusion in the gas-phase. This can easily be deduced from the definition of gas–liquid partition coefficient and Eq. (22). At this point it is helpful to analyze the case of the transport of pure water. In that case, the vapor concentration gradients within the soil are only those developed due to the reduction of the vapor pressure according to the Kelvin equation. Consequently, the diffusion of water in the gas-phase disappears if the Kelvin reduction factor is ignored within the soil and, therefore, the soil dries slower than when Kelvin effect is considered within the soil. In fact, ignoring or including the Kelvin effect within the soil is equivalent to consider or neglect the transport of water by gas-phase diffusion. This problem was studied by Chen et al. [11], who found that including the contribution of water vapor diffusion in water transport is important for improving the accuracy of water content and water flux prediction. It is noteworthy that these authors obtained differences in water content profile near the soil surface predicted when water vapor diffusion was and was not included in the water transport simulations, which are similar to the differences in volumetric liquid content shown in Fig. 11(a) caused by including or ignoring the Kelvin effect within the soil. The impact of Kelvin effect on the gas-phase diffusion fluxes of methanol and water are shown in Fig. 12. These fluxes have been normalized by the respective fluxes of volatilization and evaporation at the beginning of the volatilization period (20 h). As we can see in Fig. 12, gas-phase diffusion is significantly reduced when Kelvin effect is ignored in the model. If the Kelvin effect is considered over the entire soil, the drying process near the surface significantly reduces the liquid-phase flux and, therefore, the liquid-phase convection and dispersion. This reduction in dispersion in the liquid-phase along the first 2 cm is compensated by an increase in gas-phase diffusion in this region. When the Kelvin effect is allowed to act only at the surface, the concentration in the gas-phase within the soil is not affected by matric pressure variations and the changes in

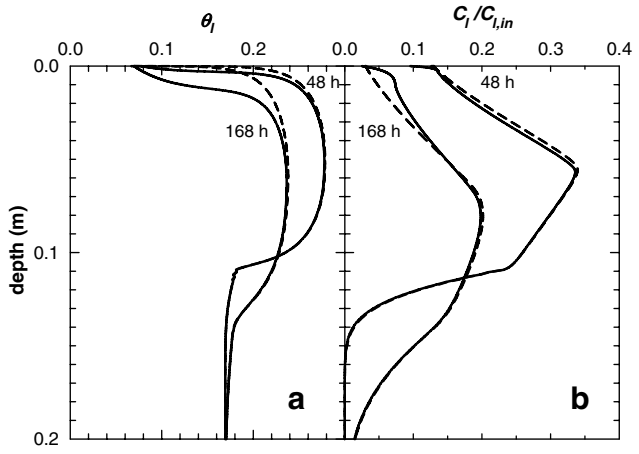

Fig. 11. Profiles after infiltration, redistribution and volatilization of a methanol–water mixture into a silty clay soil (dashed line for results ignoring Kelvin effect within the soil). (a) Volumetric liquid content, (b) methanol concentration in the liquid-phase.

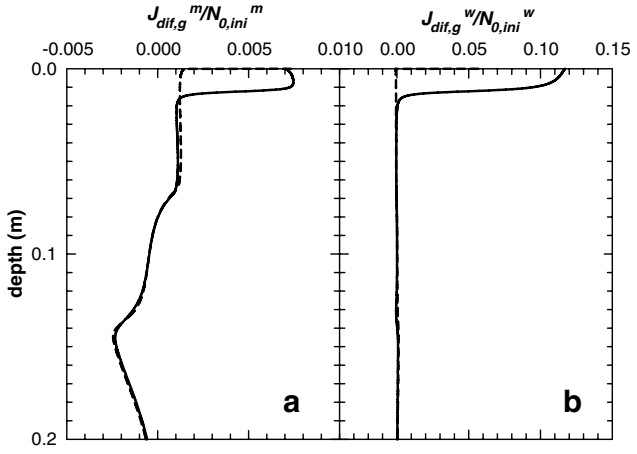

Fig. 12. Kelvin effect on normalized partial fluxes in a silty clay soil after 168 h and $C_{l,in} = 400\ kg/m^3$ (dashed line for results ignoring Kelvin effect within the soil). (a) Diffusive partial flux of methanol in the gas-phase, (b) diffusive partial flux of water in the gas-phase.

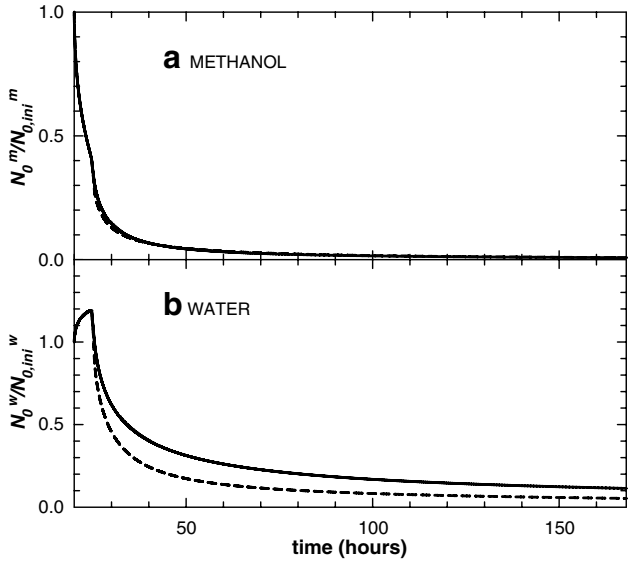

Fig. 13. Kelvin effect on methanol volatilization and water evaporation from a silty clay soil (dashed line for results ignoring Kelvin effect within the soil). (a) Volatilization of methanol, (b) evaporation of water.

concentration in the liquid-phase are insufficient to increase the gas-phase diffusion. As in this situation the liquid content is higher under relatively steep liquid concentration gradients, there are relatively high liquid-phase dispersive fluxes that at least partially compensate for the incapability of the gas-phase diffusion transport. The Kelvin effect also affected, in a similar way, the transport of water by dispersion in the liquid-phase and gas-phase diffusion.

Due to the low gas-phase diffusion of both methanol and water when the Kelvin effect is ignored within the soil, volatilization and evaporation rates are lower than the respective fluxes obtained when the Kelvin factor is considered within the soil. This situation is illustrated in Fig. 13, which shows the evolution of the methanol volatilization and water evaporation at the surface. We can see that there is a small difference in the volatilization flux of methanol but a significant one in the evaporation flux of water. Under certain conditions (clay and dry soil), therefore, there may be a great difference between considering the Kelvin effect within the soil and ignoring it. This difference is reflected in the fluxes for transport to the surface and mainly affects the less volatile compound (water, in this case).

We can conclude from this case study that the Kelvin effect plays an important role in properly representing the dynamic behavior of solute volatilization and water evaporation under high capillary pressures.

4. Conclusions

A model for the non-passive infiltration, redistribution and volatilization of liquid mixtures has been developed. It has been used to illustrate the transport of butanol and methanol aqueous solutions in the vadose zone. The coupled non-passive transport of liquid and solute through the unsaturated zone is a highly interactive phenomenon. Matric pressure gradients can induce solute transport. Reciprocally, the mixture composition may change the transport properties and induce a given pattern of flow.

Simulations for completely miscible methanol–water mixtures and two different soils (sandy clay loam and silty clay) showed significant differences in volatilization fluxes, front position, liquid content and concentration profiles that depend on the composition of the infiltrating liquid. For the cases we studied and a dispersivity value of 7.8 cm, the predominant mechanism in the transport of methanol through the soil was dispersion in the liquid-phase, with a major contribution from gas-phase diffusion near the surface during volatilization. By decomposing the liquid flux into capillary and gravity components, we found that the liquid flow is mainly due to pressure gradients induced by changes in the volumetric liquid content. However, simulations with a lower dispersivity (0.2 cm) showed that, in this case, convection was more active for methanol transport than dispersion. Also in this case, the capillary liquid flux due to changes in the composition is the predominant mechanism of liquid flow in the solute-front region.

Including or ignoring in the model the reduction of gas–liquid partition coefficients according to the Kelvin equation has an important impact on the global transport behavior. When the Kelvin effect was ignored within the soil, the gas-phase diffusion was significantly lower. The corresponding evaporation flux of water was also lower and, therefore, the volumetric liquid contents were greater. The maximum differences in the volumetric liquid content and normalized methanol concentration profiles were developed in the first 5 cm adjacent to the soil surface. These differences were increasing with time, reaching the values of 130% and 43% respectively at the end of the simulation. It was found that, under dry conditions on a silty clay soil, mass fluxes that transport the solute to the surface can be significantly different when the Kelvin factor is considered within the soil from when it is ignored. This directly affects the dynamic of solute volatilization and water evaporation rates. This phenomenon may play an important role under conditions of severe dryness, which could be crucial to accurately model the fluid flow and contaminant transport in arid regions or in clay soils, where liquid retention properties favor the development of high capillary pressures.

Acknowledgements

We gratefully acknowledge the financial assistance received from the DGICYT of Spain, under project FIS2005-07194 and from the Generalitat de Catalunya (2005SGR-00735). We also acknowledge the support received from the DURSI and the European Social Fund.

References

[1] Abbasi F, Simunek J, Feyen J, van Genuchten MTh, Shouse PJ. Simultaneous inverse estimation of soil hydraulic and solute transport parameters from transient field experiments: homogeneous soil. Trans ASAE 2003;46(4):1085–95.
[2] Allred B, Brown GO. Boundary condition and soil attribute impacts on anionic surfactant mobility in unsaturated soil. Ground Water 1996;34(6):964–71.
[3] Baggio P, Bonacina C, Schrefler BA. Some considerations on modeling heat and mass transfer in porous media. Transport Porous Med 1997;28:233–51.
[4] Bear J, Bachmat Y. Introduction to modeling of transport phenomena in porous media. Dordrecht: Kluwer; 1991.
[5] Biggar JW, Nielsen DR. Spatial variability of the leaching characteristics of a field soil. Water Resour Res 1976;1:78–84.
[6] Boufadel MC, Suidan MT, Venosa AD. Density-dependent flow in one-dimensional variably-saturated media. J Contam Hydrol 1997;202:280–301.
[7] Boufadel MC, Suidan MT, Venosa AD. A numerical model for density-and-viscosity-dependent flows in two-dimensional variably saturated porous media. J Contam Hydrol 1999;37:1–20.
[8] Brutsaert W. A theory for local evaporation (or heat transfer) from rough and smooth surfaces at ground level. Water Resour Res 1975;11(4):543–50.
[9] Burdine NT. Relative permeability calculations from pore-size distribution data. Petroleum Trans 1953;198:71–7.
[10] Chen D, Rolston DE, Yamaguchi T. Calculating partition coefficients of organic vapors in unsaturated soil and clays. Soil Sci 2000;165(3):217–25.
[11] Chen D, Rolston DE, Moldrup P. Coupling diazinon volatilization and water evaporation in unsaturated soils: I. Water transport. Soil Sci 2000;165(9):681–9.
[12] Chen D, Rolston DE. Coupling diazinon volatilization and water evaporation in unsaturated soils: II. Diazinon transport. Soil Sci 2000;165(9):690–8.
[13] Friedel MJ. Documentation and verification of VST2D. A model for simulating transient, variably saturated, coupled water-heat-solute transport in heterogeneous, anisotropic, 2-dimensional, ground-water systems with variable fluid density. US Geol. Surv. Water-Resour. Invest. Rep. 00-4105, 2000. 124 pp.
[14] Gammon BE, Marsh KN, Dewan AKR. Transport properties and related thermodynamics data of binary mixtures. Part 1. New York: American Institute of Chemical Engineers; 1993.
[15] Gawin D, Pesavento F, Schrefler BA. Modelling of hygro-thermal behaviour and damage of concrete at temperature above the critical point of water. Int J Numer Anal Meth Geomech 2002;26:537–62.
[16] Gmehling J, Onken U, Rarey-Nies JR., 1988. Vapor–liquid equilibrium data collection. Aqueous systems, vol. I, part 1b (Suppl. 2). Frankfurt: DECHEMA; 1988.
[17] Grifoll J, Cohen Y. Contaminant migration in the unsaturated soil zone: the effect of rainfall and evapotranspiration. J Contam Hydrol 1996;23:185–211.
[18] Grifoll J, Gastó JM, Cohen Y. Non-isothermal soil water transport and evaporation. Adv Water Resour 2005;28(11):1254–66.
[19] Henry EJ, Smith JE, Warrick AW. Solubility effects on surfactant-induced unsaturated flow through porous media. J Hydrol 1999;223:164–74.
[20] Henry EJ, Smith JE, Warrick AW. Surfactant effects on unsaturated flow in porous media with hysteresis: horizontal column experiments and numerical modeling. J Hydrol 2001;245:73–88.
[21] Henry EJ, Smith JE. The effect of surface-active solutes on water flow and contaminant transport in variably saturated porous media with capillary fringe effects. J Contam Hydrol 2002;56:247–70.
[22] Henry EJ, Smith JE, Warrick AW. Two-dimensional modeling of flow and transport in the vadose zone with surfactant-induced flow. Water Resour Res 2002;38(11):33-1–33-16.
[23] Henry EJ, Smith JE. Surfactant-induced flow phenomena in the vadose zone: a review of data and numerical modeling. Vadose Zone J 2003;2:154–67.
[24] Jaynes DB. Field study of bromacil transport under continuous-flood irrigation. Soil Sci Soc Am J 1991;55:658–64.
[25] Jin Y, Jury A. Characterizing the dependence of gas diffusion coefficient on soil properties. Soil Sci Soc Am J 1996;60:66–71.
[26] Kelley CT. Iterative methods for linear and nonlinear equations. Philadelphia: SIAM; 1995.
[27] Kyle BG. Chemical and process thermodynamics. New Jersey: Prentice Hall; 1999.
[28] Lenhard RJ, Oostrom M, Simmons CS, White MD. Investigation of density-dependent gas advection of trichloroethylene: experiment and a model validation exercise. J Contam Hydrol 1995;19:47–67.
[29] Leverett MC. Capillary behavior in porous solids. Trans AIME 1941;142:152–69.
[30] Lide DR, Kehiaian HV. CRC handbook of thermophysical and thermochemical data. CRC Press; 1994.
[31] Morel-Seytoux HJ, Nimmo JR. Soil water retention and maximum capillary drive from saturation to oven dryness. Water Resour Res 1999;35(7):2031–41.
[32] Nielsen DR, Biggar JW. Spatial variability of field-measured soil–water properties. Hilgardia 1973;42(7):215–59.
[33] Ouyang Y, Zheng Ch. Density-driven transport of dissolved chemicals through unsaturated soil. Soil Sci 1999;164(6):376–90.
[34] Patankar SV. Numerical heat transfer and fluid flow. New York: McGraw-Hill; 1980–1992.
[35] Press WH, Teukolsky SA, Vetterling WT, Flannery BP. Numerical recipes in Fortran 77: the art of scientific computing. New York: Cambridge University Press; 1986.
[36] Rawls WJ, Brakensiek DL. Estimation of soil water retention and hydraulic properties. Unsaturated flow in hydrology modeling, theory and practice. Kluwer Academic Publishers; 1989.
[37] Reid RC, Prausnitz JM, Poling BE. The properties of gases and liquids. New York: McGraw-Hill Inc.; 1987.
[38] Rossi C, Nimmo JR. Modeling of soil water retention from saturation to oven dryness. Water Resour Res 1994;30(3):701–8.
[39] Rowlinson JS, Widom B. Molecular theory of capillarity. Oxford: Clarendon Press; 1984.
[40] Salvucci GD. Soil and moisture independent estimation of stage-two evaporation from potential evaporation and albedo or surface temperature. Water Resour Res 1997;33(1):111–22.
[41] Schrefler BA. Multiphase flow in deforming porous material. Int J Numer Anal Meth Geomech 2004;60:27–50.
[42] Shapiro AA, Stenby EH. Kelvin equation for non-ideal multicomponent mixture. Fluid Phase Equilib 1997;134:87–101.
[43] Smith JE, Gillham RW. The effect of concentration-dependent surface tension on the flow of water and transport of dissolved organic compounds: a pressure head-based formulation and numerical model. Water Resour Res 1994;30(2):343–54.
[44] Smith JE, Gillham RW. Effects of solute concentration-dependent surface tension on unsaturated flow: laboratory sand column experiments. Water Resour Res 1999;35(4):973–82.
[45] Valsaraj KT. Elements of environmental engineering. Thermodynamics and kinetics. Boca Raton: CRC Press Inc.; 1995.
[46] White MD, Oostrom M, Lenhard RJ. Modeling fluid flow and transport in variably saturated porous media with the STOMP simulator. 1. Nonvolatile three-phase model description. Adv Water Resour 1995;18(6):353–64.
[47] White MD, Oostrom M. STOMP: Subsurface transport over multiple phases. Theory guide. PNNL-12030. Pac. Northw. Natl. Lab., Richland, WA; 2000.
[48] Zhang G, Zheng Z, Wan J. Modeling reactive geochemical transport of concentrated aqueous solutions. Water Resour Res 2005;41(W02018):1–14.